NANO LETTERS

LETTER

pubs.acs.org/NanoLett

Supported Membranes Embedded with Fixed Arrays of Gold Nanoparticles

Theobald Lohmüller,[†,§] Sara Triffo,[†] Geoff P. O'Donoghue,[†] Qian Xu,[‡] Michael P. Coyle,[†,§] and Jay T. Groves[*,†,‡,§,∥]

[†]Howard Hughes Medical Institute and Department of Chemistry and [‡]Biophysics Graduate Group, University of California, Berkeley, Berkeley, California 94720, United States

[§]Physical Biosciences and Materials Sciences Divisions, Lawrence Berkeley National Laboratory, Berkeley, California 94720, United States

[∥]Mechanobiology Institute, National University of Singapore, Singapore

Supporting Information

ABSTRACT: We present a supported membrane platform consisting of a fluid lipid bilayer membrane embedded with a fixed array of gold nanoparticles. The system is realized by preforming a hexagonal array of gold nanoparticles (~5−7 nm) with controlled spacing (~50−150 nm) fixed to a silica or glass substrate by block copolymer lithography. Subsequently, a supported membrane is assembled over the intervening bare substrate. Proteins or other ligands can be associated with the fluid lipid component, the fixed nanoparticle component, or both, providing a hybrid interface consisting of mobile and immobile components with controlled geometry. We test different biochemical coupling strategies to bind individual proteins to the particles surrounded by a fluid lipid membrane. The coupling efficiency to nanoparticles and the influence of nanoparticle arrays on the surrounding membrane integrity are characterized by fluorescence imaging, correlation spectroscopy, and super-resolution fluorescence microscopy. Finally, the functionality of this system for live cell experiments is tested using the ephrin-A1−EphA2 juxtacrine signaling interaction in human breast epithelial cells.

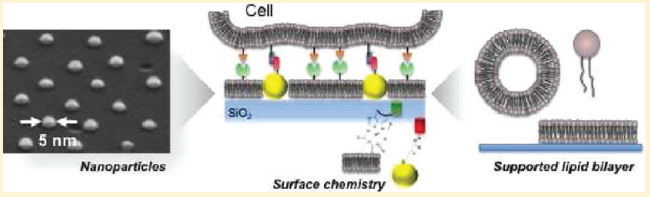

KEYWORDS: Nanoparticles, supported lipid bilayers, nanoparticle labeling, FCS, PALM

Spatial patterning of chemical and physical properties of surfaces has been used to control the behavior of cultured cells for decades.[1−7] Most of these early methods were based on patterning extracellular matrix proteins, either directly or by modulating their deposition by the cells themselves. Subsequently, more refined technologies began to focus more on specific ligand display. Such synthetically designed platforms have already provided substantial insight into how cellular functions such as adhesion,[8] migration,[9,10] proliferation,[11] differentiation,[12] as well as specific receptor activation and the role of spatial organization[13,14] are regulated on the molecular level. For example, micro- and nanopatterned arrays of adhesion molecules have been used to investigate how spatial differences of only a few nanometers can influence cell fate and response.[6] These experiments revealed that fibroblasts can apparently sense even nanoscale gradients of adhesion molecules, and underscore the precision with which cells control and react to the spatial organization of molecules.[15] While useful in many cases, immobile patterning intrinsically defeats any cellular process that naturally involves movement of the ligands, such as is particularly common among juxtacrine signaling in cell−cell junctions where both receptor and ligand reside in the fluid cell membranes.

One material platform technology that has proven particularly useful to address the more fluid nature of intercellular interactions is the supported membrane.[16] Lipid bilayers can be assembled on solid surfaces in such a way that they form a single, continuous, membrane that coats the underlying solid substrate but maintains a high degree of lateral mobility in the membrane.[16−18] Lipid mobilities in supported membranes are typically 3−4 $\mu m^2/s$, which, while several times slower than that of free bilayer membranes (e.g., in giant unilamellar vesicles[19]), is still faster than lipid mobility (~1 $\mu m^2/s$) in the crowded membranes of living cells.[20] Thus supported membranes enable ligand display along with freedom to move and reorganize naturally. Supported membranes have found productive applications in studies of the T cell immunological synapse,[21−26] neuronal interactions,[27,28] and the triggering of EphA2 receptor tyrosine kinase in breast epithelial cancer cells.[29,30] Supported membranes provide the added advantage that materials such as metals can be patterned onto the underlying substrate so as to impose fixed barriers or obstacles to mobility of molecules in the supported membrane.[21,23,24,31] Such patterned supported membranes intrinsically embody a combination of mobile and immobile characteristics, which can be used to glean insights into the function of living cells and especially the role of spatial organization and assembly in cellular processes.[32,33]

Received: August 17, 2011
Revised: September 15, 2011
Published: October 04, 2011

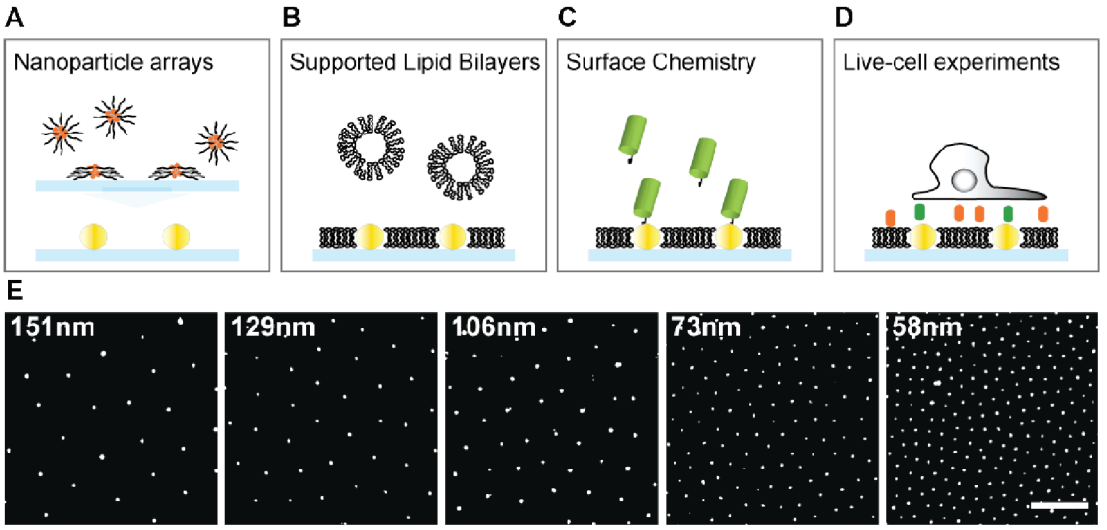

Figure 1. Schematic overview of the fabrication steps: (A) Gold nanoparticle arrays are formed by block copolymer micelle nanolithography (BCML). (B) Supported lipid bilayer formation by vesicle fusion. (C) Selective labeling of the gold nanoparticles. (D) Live-cell experiments with specific ligands bound to the nanoparticles and the lipid bilayer, respectively. (E) SEM micrographs of gold nanoparticle arrays from five different samples with individual particle spacing varying between 58 and 151 nm. The small particle size of ~5−7 nm matches the height of supported bilayer. Scale bar: 200 nm.

In this report, we describe the fabrication and characterization of a hybrid nanoparticle and supported membrane configuration consisting of an immobile array of nanoparticles embedded within a fluid supported membrane (Figure 1A−D). Nanoparticle arrays are formed by block copolymer micelle nanolithography (BCML),[34] in which nucleation sites for nanoparticle growth are first ordered by self-assembly of block copolymer micelle arrays. The organic component is subsequently plasma etched, leaving an ordered array of nanoparticles on the substrate whose spacing is dictated by the original polymer molecular weight. Key features of this system are the extraordinarily small size of the gold nanoparticles (~5−7 nm), which enables functionalization with individual protein molecules, and the controllable spacing between particles in the array in the important range of 50−150 nm, all of which are under direct synthetic control. Importantly, the BCML method of fabricating nanoparticle arrays is a self-assembly process and does not require complex patterning methods such as electron beam lithography or nanoimprint lithography.[34] Supported membranes can be assembled on these surfaces and orthogonal chemistries can be employed to functionalize the particles themselves. Fluorescence correlation spectroscopy and super-resolution microscopy are used here to examine membrane integrity and ligand coupling efficiency to the nanoparticles. Finally, application of this technology to the ephrin-A1−EphA2 signaling system in breast epithelial cells is examined as a test of its utility in a live cell format.

Nanoparticle Fabrication and Supported Lipid Bilayers. Arrays of gold nanoparticles were prepared using diblock copolymers of polystyrene(PS)-*block*-poly(2-vinylpyridine) which were dissolved in toluene. The polymer chains microphase separate into a micelle morphology with the polystyrene-block forming the outer shell and the vinylpyridine-chain forming the micellar core that can be loaded with a stoichiometric amount of a gold metal precursor. The micelles are transferred to the surface of a glass substrate by dip-coating with constant speed.[35] The sample is then treated with air plasma to remove the polymer matrix, leaving behind an array of gold nanoparticles (Figure 1E). The separation distance between the individual particles is adjustable by the molecular weight of the block copolymer and the dip-coating conditions.[35]

Supported lipid bilayers are formed by vesicle fusion from a solution of single unilamellar vesicles (SUVs).[18,36] For the experiments described here, the particle diameter was set to 7 nm, which is comparable to the thickness of the supported membrane.[37−39] Furthermore, Roiter et al. found that nanoparticles in a size range between 1.2 and 22 nm are closely surrounded by a lipid membrane instead of being covered by the bilayer.[39,40] SUVs prepared by both extrusion and probe sonication methods were used with no observable difference in the results. Representative fluorescence images, including field-stop aperture fluorescence recovery after photobleaching (FRAP),[18,41] of a supported membrane coated substrate with embedded nanoparticles is illustrated in Figure 2. The dipping edge is visible as a dark line dividing the epifluorescent image (Figure 2A, white arrow). Only the area below the dipping edge is covered with gold particles (105 nm spacing in this example); the area above corresponds to the bare glass substrate and serves as an internal reference. FRAP performed with a bleach spot straddling the dipping edge indicates comparable membrane continuity and mobility on both sides.

The influence of the nanoparticle density on the lipid diffusion was investigated in greater quantitative detail using fluorescence correlation spectroscopy (FCS).[42,43] Samples with particle spacings ranging from 58 to 151 nm were examined while keeping the particle size constant. Two different membrane systems were investigated: 0.008% TexadRed-DHPE doped bilayer of DOPC and His12-mGFP anchored to a 98.0% DOPC membrane doped with 2.00% Ni-DOGS (a DOGS lipid with a nickel-chelating, nitrilotriacetic acid (NTA) headgroup) following a previous protocol.[44] For the TexasRed lipid probe, measured diffusion coefficients were 2 $\mu m^2/s$ for all particle densities with no significant difference between the particle and the glass side (Figure 2G). The His12-mGFP exhibited diffusion coefficients ranging between

dx.doi.org/10.1021/nl202847t |*Nano Lett.* 2011, 11, 4912–4918

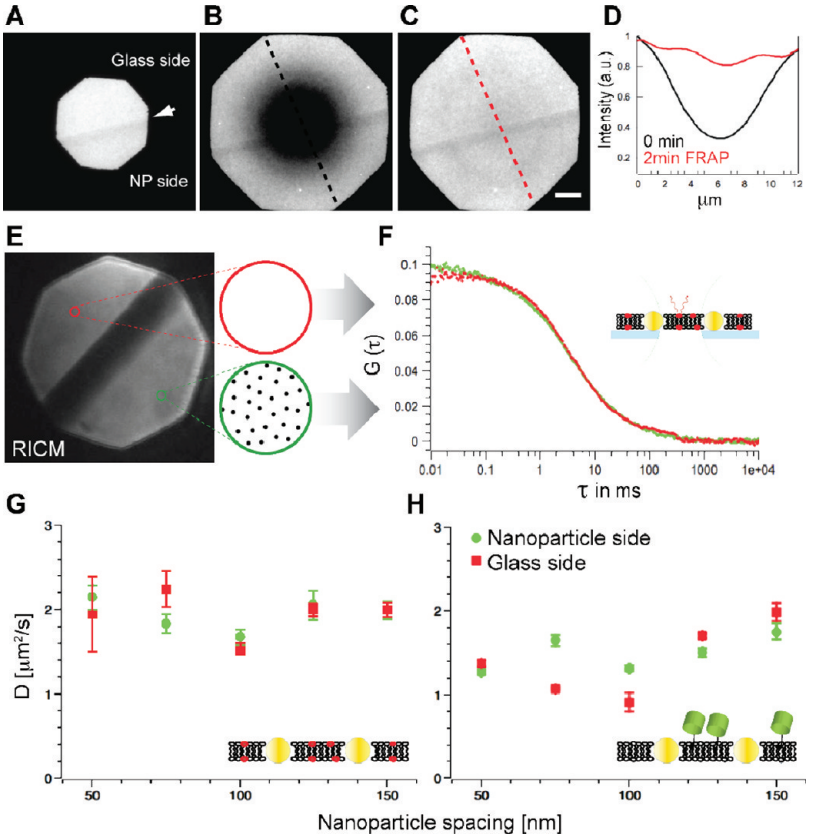

Figure 2. Probing membrane fluidity in the presence of gold nanoparticles: (A) Fluorescence recovery after photobleaching (FRAP) on a bilayer of 1,2-dioleoylphosphotidylcholine (DOPC) doped with 0.5% TexasRed-DHPE (1,2-dihexadecanoyl-*sn*-glycero-3-phosphoethanolamine, triethyl-ammonium salt): The dipping edge (white arrow) represents the borderline to where the glass substrate is covered with nanoparticles. Prior to photobleaching fluorescence is detectable on both sides of the dipping edge (top, glass side; bottom, nanoparticle side). (B) A bleached central spot is visible after illuminating the sample for 1 min with intense light. (C) After 2 min, fluorescence has recovered on both sides of the dipping edge with the same rate. (D) Line scan of the fluorescence intensity before and after 2 min displays the recovery of fluorescence. (E) RICM image of the dipping edge: FCS measurements were performed on the glass and the nanoparticle side to compare the bilayer diffusion coefficients as a function of the particle density. (F) Fluorescence correlation curves measure on the glass (red) and the nanoparticle side (green). (G, H) Diffusion coefficient as a function of the nanoparticle spacing measured by FCS: (G) DOPC bilayer doped with 0.008% TexasRed; (H) His12-mGFP anchored to the DOPC bilayer doped with 2% Ni-DOGS lipids.

1 and 2 $\mu m^2/s$ (Figure 2H) with only a small trend to faster diffusion with larger particle spacing. For a substrate with such a high density of features, we consider the possibility of significant edge effects to be a real risk.[45] Significantly, no measurable effect from area exclusion due to the nanoparticles was observed, indicating that the mobile supported membrane persists quite close to the gold nanoparticle itself, without a substantial boundary area.

Nanoparticle Functionalization Strategies and Single Molecule Fluorescence Microscopy. Four strategies were tested to bind fluorescent proteins and ligands to the gold nanoparticles embedded in a lipid bilayer (Figure 3A). Three of the linker systems tested following a two-step approach: polyhistidine−Ni^{2+}−NTA coordination chemistry,[46] *N*-hydroxysuccinimide (NHS)−ester covalent coupling,[47] and biotin−streptavidin affinity binding. For the two step approaches, thiol and disulfide linker molecules were first covalently bound to individual gold particles. In a second step, fluorescently labeled proteins were then bound to the specific linker. Double-stranded DNA with a thiol group at one 5′ end and a 6-carboxyfluorescein (FAM) group at the 5′ end of the complementary strand was used to functionalize the nanoparticles in a single step. For all methods, successful coupling was characterized by fluorescence microscopy (Figure 3B). Fluorescence was observed only on the nanoparticle; negligible fluorescence was observed off the nanoparticle arrays or in control experiments without linker molecules.

Comparing all four methods, His-tag-Ni^{2+}/NTA coupling proved most advantageous as it allows site-specific protein immobilization with high binding affinity and control over the binding orientation. However, the method suffers from unbinding over time due to instability of the Ni(II)-coordinating complex.[44] Alternatively, *N*-hydroxysuccinimide (NHS) esters can bind to primary amines from proteins forming a covalent amide bond. However, protein labeling is not site-selective, which could jeopardize the protein functionality. In addition, NHS suffers from unwanted side-reactions with water molecules in aqueous solution. Biotin−streptavidin is a popular strategy of creating high affinity linkages, but this is not site-selective and the multivalency of streptavidin as well as its intrinsic tendency to oligomerize creates an avenue for aggregation. Indeed, we observe large fluorescent aggregates for biotin coupling (Figure 3B). DNA offers many benefits for anchoring proteins, including especially its potential for massive orthogonality. In addition the length and flexibility of the DNA molecules can be tuned as needed. These are not examined in detail here.

dx.doi.org/10.1021/nl202847t |*Nano Lett.* 2011, 11, 4912–4918

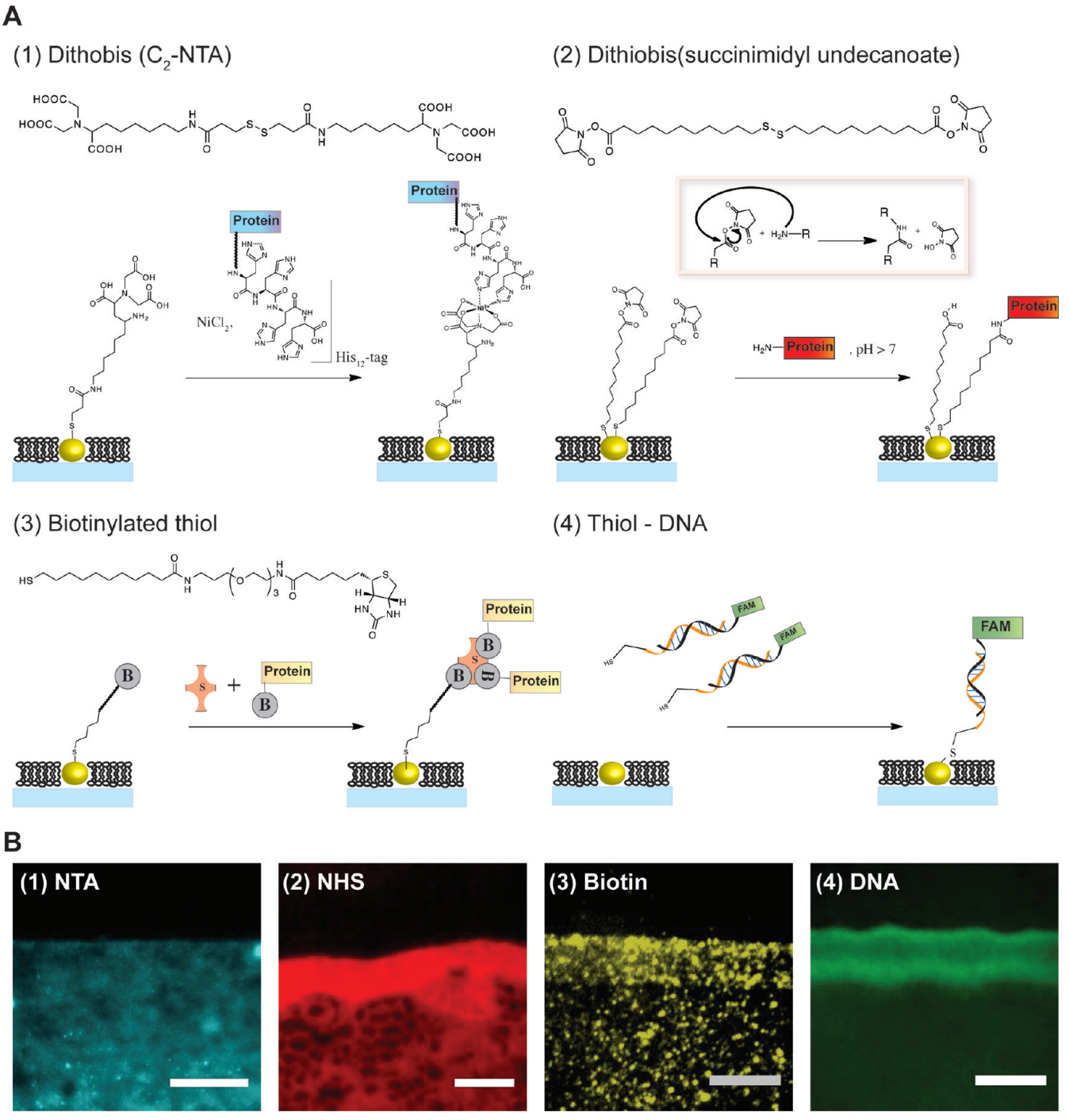

Figure 3. (A) Overview on functionalization strategies for gold nanoparticles in the presence of a lipid bilayer: (1) Coupling of His-tagged molecules to gold nanoparticles via Ni(II)-coordinating NTA-thiol linker molecules. (2) *N*-Hydroxysuccinimide (NHS) coupling of proteins: The succinimidylesters group reacts with primary amines from proteins by forming a stable amide bond (figure inset). Since NHS is a good leaving group, hydrolysis of the activated ester occurs as a side reaction in water. (3) Biotin−streptavidin affinity binding: Biotin−thiol linker molecules are bound to the particles in buffer solution. Biotin-functionalized proteins are attached via biotin−streptavidin coupling. Streptavidin displays four binding sites to bind biotinylated proteins. (4) Labeling with thiolated-DNA with a thiol group at one 5′ end and a 6-carboxyfluorescein (FAM) group at the 5′ end of the complementary strand. (B) Epifluorescence images of immobilized fluorescent labeled proteins bound to gold nanoparticles. Scale bars: 5 μm.

Protein coupling to individual nanoparticles was analyzed by photoactivated localization microscopy (PALM).[48,49] For this study, ephrinA1-mEos-His10 fusion proteins were attached to the gold nanoparticles using Ni(II)-coordinating NTA coupling as described above. The photoactivatable fluorescent protein (PAFP) mEos2 is suitable for PALM experiments because it irreversibly isomerizes from a green to a red fluorescent state upon irradiation with UV light and to date has one of the highest photon yields and highest contrast between bright and dark fluorescent states of all PAFPs.[50] Individual mEos2 molecules

dx.doi.org/10.1021/nl202847t |*Nano Lett.* 2011, 11, 4912–4918

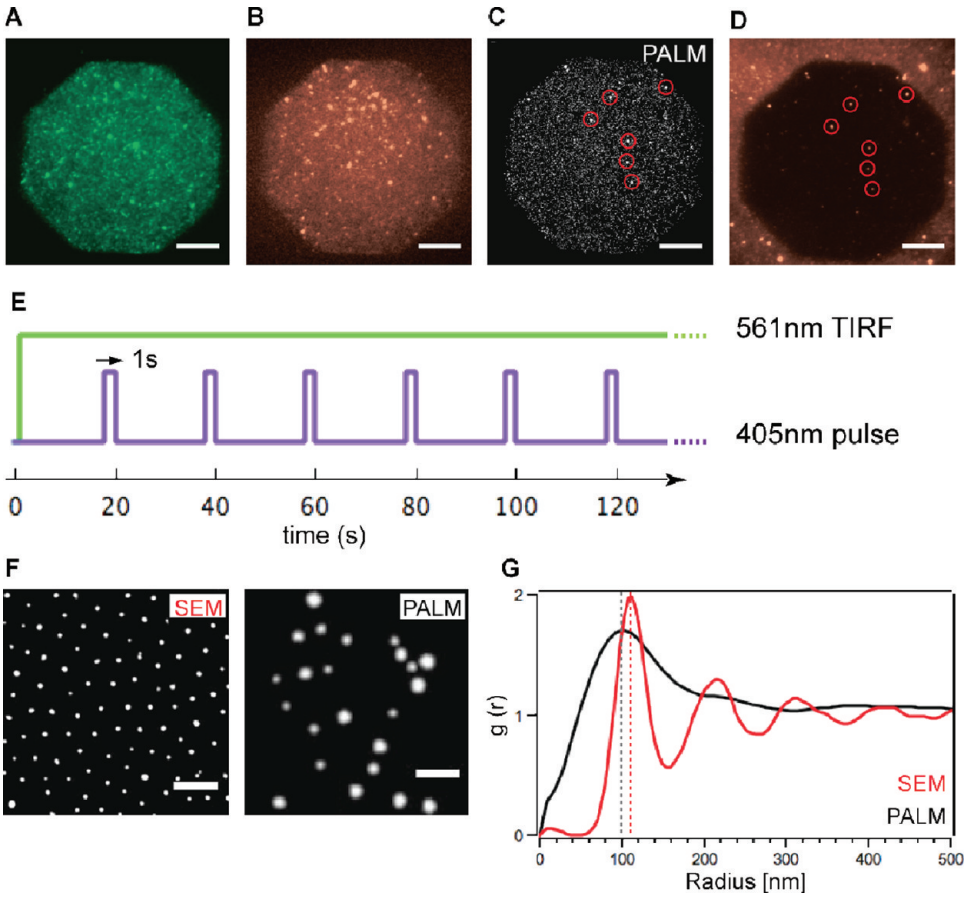

Figure 4. PALM imaging of ephrin-mEos-His10 anchored to gold nanoparticles: (A) TIRF image using 488 nm illumination (green fluorescent state). (B) TIRF image of the same area as in (A) using 561 nm illumination with the field diaphragm fully open after intense activation pulse using 405 nm TIRF illumination (red fluorescent state). After activation with the 405 pulse the TIRF image using 561 nm illumination shows that only molecules within the field diaphragm were activated while those on the outside are not activated and therefore dark under 561 nm illumination. (C) PALM image of the fluorescent molecules. (D) At laser powers of 20−30 mW, 561 nm, and 0.1−1 mW, 405 nm, both measured at the sample, the field of view showed complete depletion of fluorescence after approximately 30 min using 100 ms exposure times and stream acquisition. Defects from the nanoparticle array are visible in both the PALM and 561 TIRF images (red circles). (E) Schematic of the laser illumination sequence. Individual mEos2 molecules were activated using a 405 nm laser pulse for 1 s in 20 s increments while continuously imaging the sample with a 561 nm laser in TIRF mode. (F, right) Close-up of individual molecules detected by PALM and (F, left) reference SEM image of the same sample. Scale bar is 200 nm in both cases. (G) Comparison of the radial distribution function from the full PALM image (black) and the reference SEM image (red).

were activated using a 405 nm laser pulse for 1 s in 20 s increments while continuously imaging the sample until the field of view showed complete depletion (Figure 4D). Small defects were observed where the mEOS could not be bleached over the course of the data acquisition (Figure 4C,D). These spots are likely caused by contaminations and defects on the glass substrate that lead to particle agglomerations or holes in the bilayer itself. PALM images were constructed according to Gould et al.[51] The nearest neighbor distance of fluorescent molecules from the PALM rendered image was compared to the particle spacing from a reference SEM micrograph by calculating the radial distribution functions $g(r)$[52] (Figure 4G). A molecule spacing of approximately 100 nm was calculated for the full PALM image, which is in good agreement with the data calculated from SEM imaging of the nanoparticles themselves (~110 nm). The coupling yield of mEos2 molecules to individual gold particles was found to be 24% by comparing the number of gold nanoparticles measured by SEM with the number of fluorophores localized with PALM. It has to be noted that the overall number of detected particles depends on several experimental parameters such as the labeling yield of the NTA linker to the gold particles, the labeling yield of the mEOS2 to the linker, the absolute number or active/inactive mEOS2 molecules, and the efficiency of the PALM readout. No particles were lost due to the functionalization process as verified by SEM (Supporting Information).

Live Cell Experiments. Live cell experiments were performed with MDA-MB-231 cells, a highly invasive human breast epithelial cancer cell line.[53] This particular cell line is known for overexpressing the EphA2 receptor tyrosine kinase that interacts with its biological ligand, ephrin-A1, in juxtracrine fashion and has been used in previous studies by our group.[29,30] The cells do not exhibit any nonspecific interaction with the control substrates consisting of unfunctionalized nanoparticles or of nanoparticles functionalized with NTA-linker molecules only (Figure 5A). In contrast, prolific adhesion was observed on the nanoparticle side of the substrate (Figure 5B). In a contrasting experiment, cells were exposed to a substrate in which the membrane was doped in an RGD (arginine−glycine−asparatic acid) motif bound to a mobile lipid. RGD is a peptide sequence that is found in extracellular matrix proteins and known to promote integrin-mediated cell adhesion.[54]

dx.doi.org/10.1021/nl202847t |*Nano Lett.* 2011, 11, 4912–4918

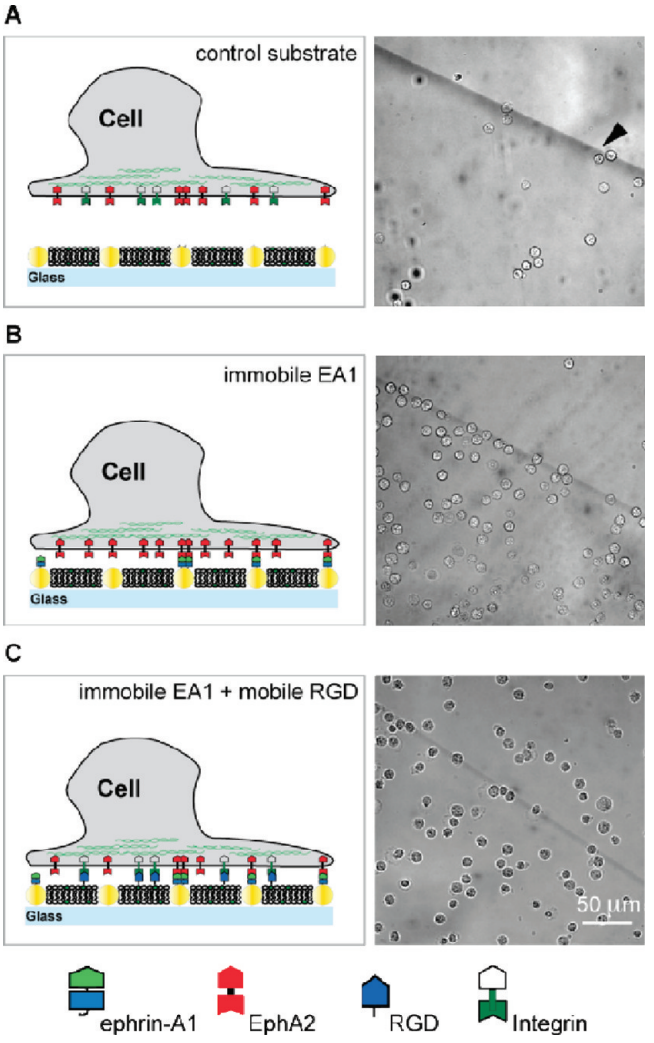

Figure 5. Human breast cancer MDA-MB-231 cells expressing the EphA2 receptor tyrosine kinase are cultured on the nanoparticle/supported bilayer substrate. After 1 h of incubation on the surface, the cells were fixed and imaged using brightfield illumination microscopy. (A) On the nonfunctionalized substrate without any ligand protein, ephrin-A1, the brightfield image shows a mostly bare surface with very few cells that are nonspecifically attached to defects in the glass. (B) On the surface that is only displaying immobile ephrin-A1 ligand protein, functionalized on the nanoparticles, surrounded by a bilayer containing 100% DOPC, the cells selectively bind to the nanoparticle side on the substrate and line up along the dipping edge. (C) When the integrin-interacting peptide, arginine−glycine−asparatic acid (RGD) is anchored to the lipid bilayer, the cells can interact with both sides of the dipping edge. RGD peptides were labeled with biotin and then bound to the biotin lipids on the bilayer through a streptavidin linker (the biotin lipids consist of 99.9% DOPC and 0.1% biotin-DPPE).

In this experiment, both the bilayer and the nanoparticles were functionalized with molecules that promote cell adhesion and the cells were found all over the substrate (Figure 5C).

These results are the first example of an advanced platform of fixed gold nanoparticle arrays and supported lipid bilayers for biological studies. This new strategy that combines fixed nanopatterning with the mobility of fluid supported lipid bilayers is an important improvement over previous methods that use strictly mobile or strictly static protein patterning and offers great potential for future studies of living cells.

■ ASSOCIATED CONTENT

Supporting Information. A Materials and Methods section describing the experimental procedures and instrument setups. This material is available free of charge via the Internet at http://pubs.acs.org.

■ AUTHOR INFORMATION

Corresponding Author
*E-mail: jtgroves@lbl.gov.

■ ACKNOWLEDGMENT

Research supported by the U.S. Department of Energy, Office of Basic Energy Sciences, Division of Materials Sciences and Engineering and the Molecular Foundry, Lawrence Berkeley National Laboratory. The authors acknowledge Adam W. Smith, Hector Huang, Niña Hartman, Boryana Manz, and Pradeep Nair for fruitful discussions and experimental reagents. The authors would like to thank Sam Hess for providing his PALM analysis code. Theobald Lohmüller was supported by a postdoc fellowship from the Deutsche Forschungsgemeinschaft (DFG).

■ REFERENCES

(1) Kleinfeld, D.; Kahler, K.; Hockberger, P. *J. Neurosci.* **1988**, *8* (11), 4098–4120.
(2) Clark, P.; Britland, S.; Connolly, P. *J. Cell Sci.* **1993**, *105*, 203–212.
(3) Singhvi, R.; Kumar, A.; Lopez, G. P.; Stephanopolous, G. N.; Wang, D. I. C.; Whitesides, G. M.; Ingber, D. E. *Science* **1994**, *264*, 696–698.
(4) Healy, K. E.; Lom, B.; Hockberger, P. E. *Biotechnol. Bioeng.* **1994**, *43*, 792–800.
(5) Mrksich, M.; Chen, C. S.; Xia, Y.; Dike, L. E.; Ingber, D. E.; Whitesides, G. *Proc. Natl. Acad. Sci. U.S.A.* **1996**, *93*, 10775–10778.
(6) Chen, C. S.; Mrksich, M.; Huang, S.; Whitesides, G. M.; Ingber, D. E. *Science* **1997**, *276* (5317), 1425–1428.
(7) Takayama, S.; McDonald, J. C.; Ostuni, E.; Liang, M. N.; Kenis, P. J. A.; Ismagilov, R. F.; Whitesides, G. M. *Proc. Natl. Acad. Sci. U.S.A.* **1999**, *96*, 5545–5548.
(8) Arnold, M.; Cavalcanti-Adam, A.; Glass, R.; Blümmel, J.; Eck, W.; Kessler, H.; Spatz, J. P. *ChemPhysChem* **2004**, *4*, 872–877.
(9) Koo, L. Y.; Irvine, D. J.; Mayes, A. M.; Lauffenburger, D. A.; Griffith, L. G. *J. Cell Sci.* **2002**, *115*, 1423–1433.
(10) Cavalcanti-Adam, E. A.; Micoulet, A.; Blümmel, J.; Auernheimer, J.; Kessler, H.; Spatz, J. P. *Eur. J. Cell Biol.* **2005**, *85* (3−4), 219–224.
(11) Yima, E. K. F.; Reanob, R. M.; Pangb, S. W.; Yeec, A. F.; Chena, C. D.; Leong, K. W. *Biomaterials* **2005**, *26* (26), 5405–5413.
(12) Yim, E.; Pang, S.; Leong, K. *Exp. Cell Res.* **2007**, *313* (9), 1820–1829.
(13) Doh, J.; Irvine, D. J. *Proc. Natl. Acad. Sci. U.S.A.* **2006**, *103* (15), 5700–5705.
(14) Irvine, D. J.; Doh, J.; Huang, B. *Curr. Opin. Immunol.* **2007**, *19*, 463–469.
(15) Arnold, M.; Hirschfeld-Warneken, V.-C.; Lohmueller, T.; Heil, P.; Bluemmel, J.; Cavalcanti-Adam, E.-A.; Lopez-Garcia, M.; Walther, P.; Kessler, H.; Geiger, B.; Spatz, J. P. *Nano Lett.* **2008**, *8* (7), 2063–2069.
(16) Sackmann, E. *Science* **1996**, *271* (5245), 43–48.
(17) Groves, J. T.; Boxer, S. G. *Acc. Chem. Res.* **2002**, *35*, 149–157.
(18) Lin, W.-C.; Yu, C.-H.; Triffo, S.; Groves, J. T. *Curr. Protoc. Chem. Biol.* **2010**, *2*, 235–269.
(19) Kahya, N.; Scherfeld, D.; Bacia, K.; Schwille, P. *J. Struct. Biol.* **2004**, *147* (1), 77–89.
(20) Schwille, P.; Haupts, U.; Maiti, S.; Webb, W. W. *Biophys. J.* **1999**, *77*, 2251–2265.

(21) Manz, B. N.; Jackson, B. L.; Petit, R. S.; Dustin, M. L.; Groves, J. T. *Proc. Natl. Acad. Sci. U.S.A.* **2011**, *108* (22), 9089–9094.
(22) Grakoui, A.; Bromley, S. K.; Sumen, C.; Davis, M. M.; Shaw, A. S.; Allen, P. M.; Dustin, M. L. *Science* **1999**, *285* (5425), 221–227.
(23) Mossman, K.; Groves, J. *Chem. Soc. Rev.* **2007**, *36* (1), 46–54.
(24) DeMond, A. L.; Mossman, K.; Starr, T.; Dustin, M. L.; Groves, J. T. *Biophys. J.* **2008**, *94* (8), 3286–3292.
(25) Hartman, N. C.; Nye, J. A.; Groves, J. T. *Proc. Natl. Acad. Sci. U.S.A.* **2009**, *106* (31), 12729–12734.
(26) Groves, J. T.; Dustin, M. *J. Immunol. Methods* **2003**, 19–32.
(27) Baksh, M. M.; Dean, C.; Pautot, S.; DeMaria, S.; Isacoff, E.; Groves, J. T. *Langmuir* **2005**, *21* (23), 10693–10698.
(28) Pautot, S.; Lee, H.; Isacoff, E. Y.; Groves, J. T. *Nat. Chem. Biol.* **2005**, *1*, 283–289.
(29) Salaita, K.; Nair, P. M.; Petit, R. S.; Neve, R. M.; Das, D.; Gray, J. W.; Groves, J. T. *Science* **2010**, *327*, 1380–1385.
(30) Xu, Q.; Lin, W.-C.; Petit, R. S.; Groves, J. T. *Biophys. J.* **2011**, in review.
(31) Groves, J. T.; Ulman, N.; Boxer, S. G. *Science* **1997**, *275*, 651–653.
(32) Manz, B. N.; Groves, J. T. *Nat. Rev. Mol. Cell Biol.* **2010**, *11* (5), 342–352.
(33) Groves, J. T.; Kuryan, J. *Nat. Struct. Mol. Biol.* **2010**, *17*, 659–665.
(34) Glass, R.; Moeller, M.; Spatz, J. P. *Nanotechnology* **2003**, *14*, 1153–1160.
(35) Lohmueller, T.; Aydin, D.; Schwieder, M.; Morhard, C.; Louban, I.; Pacholski, C.; Spatz, J. P. *Biointerphases* **2011**, *6* (MR1), 12.
(36) Richter, R. P.; Bérat, R.; Brisson, A. R. *Langmuir* **2006**, *22*, 3497–3505.
(37) Lohmueller, T.; Bock, E.; Spatz, J. P. *Adv. Mater.* **2008**, *20*, 2297–2302.
(38) Goksu, E. L.; Vanegas, J. M.; Blanchette, C. D.; Lin, W.-C.; Longo, M. L. *Biochim. Biophys. Acta, Biomembr.* **2008**, *1788* (1), 254–266.
(39) Roiter, Y.; Ornatska, M.; Rammohan, A. R.; Balakrishnan, J.; Heine, D. R.; Minko, S. *Langmuir* **2009**, *25* (11), 6287–6299.
(40) Roiter, Y.; Ornatska, M.; Rammohan, A. R.; Balakrishnan, J.; Heine, D. R.; Minko, S. *Nano Lett.* **2008**, *8* (3), 941–944.
(41) Salafsky, J.; Groves, J. T.; Boxer, S. G. *Biochemistry* **1996**, *35* (40), 14773–14781.
(42) Groves, J. T.; Parthasarathy, R.; Forstner, M. B. *Annu. Rev. Biomed. Eng.* **2008**, *10*, 311–338.
(43) Forstner, M. B.; Yee, C. K.; Parikh, A. N.; Groves, J. T. *J. Am. Chem. Soc.* **2006**, *128* (47), 15221–15227.
(44) Nye, J. A.; Groves, J. T. *Langmuir* **2008**, *24* (8), 4145–4149.
(45) Smith, A. M.; Vinchurkar, M.; Gronbech-Jensen, N.; Parikh, A. N. *J. Am. Chem. Soc.* **2010**, *132* (27), 9320–9327.
(46) Wolfram, T.; Belz, F.; Schön, T.; Spatz, J. P. *Biointerphases* **2007**, *2*, 44–48.
(47) Cline, G. W.; Hanna, S. B. *J. Org. Chem.* **1988**, *53*, 3583–3586.
(48) Betzig, E.; Patterson, G. H.; Sougrat, R.; Lindwasser, O. W.; Olenych, S.; Bonifacino, J. S.; Davidson, M. W.; Lippincott-Schwartz, J.; Hess, H. F. *Science* **2006**, *313* (5793), 1642–1645.
(49) Hess, S. T.; Girirajan, T. P. K.; Mason, M. D. *Biophys. J.* **2006**, *91* (11), 4258–4272.
(50) McKinney, S. A.; Murphy, C. S.; Hazelwood, K. L.; Davidson, M. W.; Looger, L. L. *Nat. Methods* **2009**, *6*, 131–133.
(51) Gould, T. J.; Verkhusha, V. V.; Hess, S. T. *Nat. Protoc.* **2009**, *4*, 291–308.
(52) Reichl, L. E. *A Modern Course in Statistical Physics*, 3rd Revised and Updated ed.; Wiley-VCH: Weinheim, 2009.
(53) Neve, R. M.; Chin, K.; Fridlyand, J.; Yeh, J.; Baehner, F. L.; Fevr, T.; Clark, L.; Bayani, N.; Coppe, J.-P.; Tong, F.; Speed, T.; Spellman, P. T.; DeVries, S.; Lapuk, A.; Wang, N. J.; Kuo, W.-L.; Stilwell, J. L.; Pinkel, D.; Albertson, D. G.; Waldman, F. M.; McCormick, F.; Dickson, R. B.; Johnson, M. D.; Lippman, M.; Ethier, S.; Gazdar, A.; Gray, J. W. *Cancer Cell* **2006**, *10* (6), 515–527.
(54) Geiger, B.; Spatz, J. P.; Bershadsky, A. D. *Nat. Rev. Mol. Cell Biol.* **2009**, *10* (1), 21–33.